Transient Vibrational Echo versus Transient Absorption Spectroscopy: A Direct Experimental and Theoretical Comparison

CARLOS R. BAIZ, ROBERT McCANNE, and KEVIN J. KUBARYCH*

Department of Chemistry, University of Michigan, Ann Arbor, Michigan 48109

Transient dispersed vibrational echo (DVE) spectroscopy is a practical alternative to transient-absorption spectroscopy because it affords increased sensitivity as well as greater signal-to-noise ratio without the need to detect a reference spectrum. However, as a third-order nonlinear probe, the extraction of kinetic information from transient-DVE is somewhat cumbersome compared to transient absorption. This article provides a direct experimental and theoretical comparison between transient-absorption and transient-DVE measurements and presents a framework for analyzing kinetic measurements while exploring the implications of making some simplifying assumptions in the data analysis. The equations for computing the signal-to-noise ratios under different experimental conditions are derived and used in the analysis of the experimental data. The results, obtained under the same experimental conditions, show that for a relatively strong terminal carbonyl stretching mode, signal-to-noise ratios in transient-DVE spectroscopy are approximately 2.5 times greater than transient absorption. The experimental results along with the theoretical models indicate that transient-DVE could become an attractive alternative to transient-absorption spectroscopy for measuring the kinetics of light-induced processes.

Index Headings: **Transient; Vibrational echo; Ultrafast; Infrared spectroscopy; Nonlinear spectroscopy.**

INTRODUCTION

Time-resolved vibrational spectroscopy provides information on transient molecular processes by allowing the direct measurement of the vibrational frequencies in a chemical system during a non-equilibrium process. Ultrafast infrared and visible spectroscopy have been used to elucidate the dynamics of many fundamental processes including alpha-helix formation in peptides,[1,2] hydrogen bond dynamics,[3–7] and ligand photodissociation in proteins.[8–10] The well-established method of transient infrared absorption spectroscopy (TA) consists of monitoring the infrared absorption spectrum of a system as a function of the time delay after an event, usually a photochemical or photophysical process initiated by a laser pulse.[11] This technique is relatively straightforward to implement and the data can provide rich structural and dynamical information such as reaction rates or orientational lifetimes.[12,13] Though TA can provide high time resolution of transient processes, the spectral measurement is one dimensional (1D) and is thus limited in its dynamical information content. To circumvent the inherent limitations of 1D spectroscopy, multidimensional techniques have now gained wide adoption.[14–17] Coherent two-dimensional infrared (2D-IR) spectroscopy, a third-order nonlinear technique, offers a direct measurement of the full vibrational Hamiltonian, including anharmonicities and couplings,[18–20] while providing a separation between inhomogeneous and homogeneous broadening. 2D-IR effectively spreads the infrared spectrum onto two axes, corresponding to excitation and detection frequencies, and the dynamics are contained in the dependence of peak amplitudes on the time delay between excitation and detection as well as the peak line shapes, whereas structural information is generally contained in the off-diagonal peak amplitudes.[21–23]

To date, the majority of 2D-IR measurements have been made on systems at equilibrium that are minimally perturbed by the infrared excitation.[24] Molecular spectral line shapes are determined by a combination of dynamic and static microscopic origins, and a 1D spectrum cannot distinguish these different contributions without making significant assumptions, which may be unwarranted. For example the time scale on which a system samples an inhomogeneous distribution of distinct microenvironments cannot be extracted from 1D spectra, but it arises naturally in 2D spectroscopy. Similarly obscured in a 1D spectrum is the coupling between transitions within a molecule, information that is easily deduced from cross-peak patterns in 2D spectra. This latter capability, which is similar to the powerful features of multidimensional NMR spectroscopy, has been exploited in several analytical applications of 2D-IR spectroscopy.[25–27] In a sense, 2D-IR spectroscopy is an "optical separation," since cross-peaks are typically not observed between different types of molecules present in the same sample. For example, 2D-IR has been used to identify mixtures of proteins using a kind of 2D barcode based on the specific two-dimensional coupling pattern in the measured 2D-IR spectrum.[27] A key advantage of the separation ability of 2D-IR spectroscopy is its inherent ultrafast (sub-picosecond) time resolution.

Two-dimensional infrared spectroscopy has been extended to the non-equilibrium regime, either by optically perturbing the system before the 2D-IR measurement (transient-2D-IR) or during the waiting time period (triggered-exchange 2D-IR).[28–31] The first technique is the two-dimensional equivalent of transient absorption while the second technique provides a correlation between the vibrational frequencies in the system before and after the perturbation. Since transient 2D-IR spectroscopy is a time-consuming method, and is subject to slow drift in the experimental apparatus, often it is desirable to track reactions using a 1D probe to extract kinetic information, while relying upon a few transient 2D-IR spectra in order to extract dynamics or to assign the 1D spectrum.[32,33]

In this paper, we consider nonlinear dispersed vibrational echo (DVE) spectroscopy, in the context of 2D-IR spectroscopy, as a sensitive probe of chemical kinetics and compare it to the well-established transient-absorption spectroscopy. The experimental and theoretical comparison is approached from a practical perspective, considering issues such as signal intensities and

Received 23 February 2010; accepted 3 June 2010.

* Author to whom correspondence should be sent. E-mail: kubarych@umich.edu.

0003-7028/10/6409-1037$2.00/0

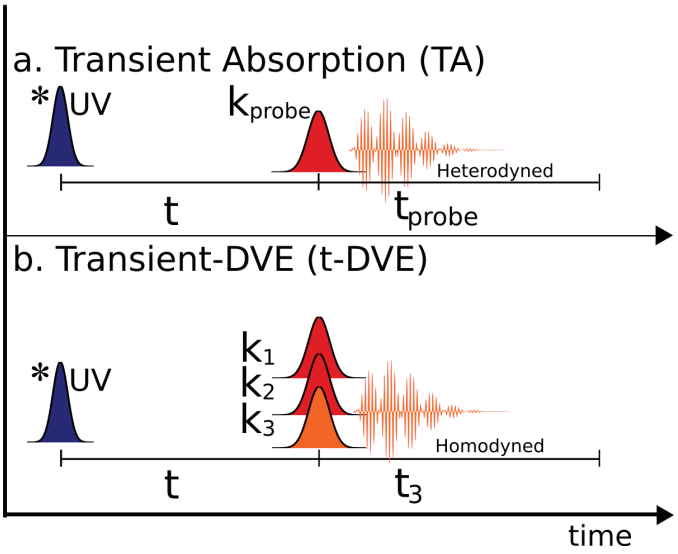

FIG. 1. Pulse sequence used for (**a**) transient absorption and (**b**) transient-DVE measurements. The UV pulse is chopped to half the laser repetition rate and a differential signal is recorded.

noise fluctuations, while providing a framework for obtaining kinetic information such as reaction rates and quantum yields from transient-DVE measurements. In addition, we derive the equations needed for estimating the signal-to-noise ratios for transient-DVE and TA under different experimental conditions.

VIBRATIONAL ECHO SPECTROSCOPY

A vibrational echo experiment is carried out by applying three non-collinear infrared pulses resonant with a molecular transition and measuring an emitted signal—or vibrational echo—in a phase-matched direction. For a simple one-oscillator system, the experiment can be described as follows: The first pulse creates a coherent superposition between the ground ($\nu = 0$) and first-excited ($\nu = 1$) vibrational levels of the specific mode. The second incoming pulse creates a population in either the ground or first excited state depending on the phase-difference with respect to the first pulse. The third pulse finally puts the sample back into a coherent superposition between the ground and first excited states and between the first and second excited states. The final superposition results in an oscillating dipole, which then radiates at either the $\nu = 0 \rightarrow 1$ or the $\nu = 1 \rightarrow 2$ transition frequencies. The emitted signal is usually measured using a conventional grating spectrometer. The anharmonicity of the mode dictates the difference between the $\nu = 0 \rightarrow 1$ and $\nu = 1 \rightarrow 2$ transition frequencies. From a molecular structure perspective, vibrational echo spectroscopy provides a direct measure of the normal-mode anharmonicity, a measurement that cannot be obtained from linear absorption spectroscopy. If the system contains multiple infrared-active modes, signal contributions can be observed from anharmonic transitions involving two different modes. Detailed descriptions of vibrational echo spectroscopy, including line shape comparisons and the effects of concentration and oscillator strength on the signal amplitude, have been presented elsewhere.[34] Finally, due to the nonlinear nature of the light–matter interaction the vibrational echo signal arising from a low concentration of strong absorbers generally dominates the signal due to a high concentration of weak absorbers.[34] This selectivity for transitions with strong transition dipole moments was recently illustrated very clearly in a study of a dye-sensitized semiconductor system.[31] Typical transient IR absorption measurements contain a very large and relatively uninformative continuum absorption due to free electrons in the semiconductor. In the transient 2D-IR measurements, however, the free-carrier continuum was not present in the two-dimensional plots. Suppression of low-oscillator-strength background signals, like sensitivity to anharmonicity, is another advantage of t-DVE that is separate from signal-to-noise ratio considerations.

In general, two-dimensional infrared spectra are measured using two different experimental approaches: time-domain Fourier transform (FT) 2D-IR, or frequency-resolved dynamic hole burning (frequency-domain) 2D-IR. In principle, both techniques provide identical information, but practical differences limit the information provided by hole-burning at early waiting times. A thorough comparison between the two methods has been published previously.[35] In the case of background-free FT-2D-IR, three IR pulses are applied to the sample and the amplitude and phase of the echo signal are measured by interferometry with a reference pulse in a spectrometer.[23] One feature of the Fourier transform approach is that by time-overlapping the three IR pulses and blocking the reference pulse, one obtains a dispersed vibrational echo spectrum. The pulse sequences for TA and transient-DVE are shown in Fig. 1. A DVE spectrum corresponds to the square of the projection of the 2D-IR spectrum on to the detection axis. The DVE signal, which arises from the same pulse interactions as the 2D-IR signal, can provide structural information not available in a one-dimensional absorption spectrum. The most notable difference between DVE and TA is DVE's sensitivity to vibrational anharmonicity. Similar to 2D-IR, the DVE measurements can also be performed on a non-equilibrium system by applying an extra laser pulse before the three infrared pulses: transient-DVE (or t-DVE) spectroscopy. This technique yields similar information to TA spectroscopy, but because t-DVE is a nonlinear probe, the data analysis can be somewhat more complicated than TA.

Recently, Jones and co-workers[36] demonstrated the use of heterodyne-detected vibrational echo (HDVE) spectroscopy as a method to characterize non-equilibrium dynamics and compared it to DVE and TA. Similar to 2D-IR, an HDVE spectrum is obtained by interferometric superposition of the signal with an external reference pulse. One of the key advantages of HDVE lies in its ability to separate the absorptive and diffractive components of the molecular response function. Although as an interferometric method, HDVE has the ability to amplify weak signals by using a strong reference, which can be advantageous when working with weak absorbers or low concentrations, the presence of a strong reference pulse in HDVE greatly reduces the dynamic detection range. Homodyne detected DVE, on the other hand, is a background-free method that is able to make use of the entire dynamic range of the detector.

In a recent publication,[37] we employed transient-2D-IR and transient-DVE, to measure the asymmetric rebinding of cyclopentadienylmolybdenum(II) tricarbonyl dimer, a dimetal carbonyl molecule that exists in two different isomer conformations *trans*, and *gauche*. The equilibrium constant of the two isomers, $K_{G/T}$, is approximately 0.25 in polar solvents with interconversion occurring in the millisecond

timescale.[38] Each isomer has distinct terminal-carbonyl absorption bands in the infrared, thus providing kinetic information in a structure-specific manner. Upon absorption of a 400-nm photon, both isomers undergo photocleavage of the metal–metal bond to generate two solvent-caged monomers.[39–41] By monitoring the transient-DVE bleach recovery associated with the *trans* and *gauche* conformations, we were able to conclude that rebinding exclusively favors the *trans* isomer.[37] The study highlighted structural sensitivity as one of the main strengths of vibrational spectroscopy, which is usually not afforded by electronic spectroscopy. This geminate recombination reaction will be used to test and compare t-DVE and TA as described in the next section.

THEORETICAL MODELS

Several different theoretical approaches to computing a nonlinear infrared spectrum of a given molecular system have been developed (see Ref. 42 and references therein). In this work, we use the standard perturbative approach in which the polarization giving rise to the signal is computed as a convolution between the system's optical response function, $S^{(3)}(t_1, t_2, t_3)$, and the applied laser fields:

$$P^{(3)}(t) = \int_0^\infty \mathrm{d}t_3 \int_0^\infty \mathrm{d}t_2 \int_0^\infty \mathrm{d}t_1 S^{(3)}(t_1, t_2, t_3) E_3(t - t_3) \times E_2(t - t_3 - t_2) E_1(t - t_3 - t_2 - t_1) \quad (1)$$

To simulate the experimental transient-DVE data presented below, we start with a third-order optical response function for a one-dimensional anharmonic oscillator in the molecular frame so that contributions due to orientational relaxation are neglected. The modeling is done within the context of Redfield theory with a phenomenological dephasing rate.[43] The main input parameters are the oscillator strengths for the lowest two transitions, V_{10} and V_{21}, and the transition frequencies, ω_{10}, and ω_{21}. The relaxation parameters represent the decays of diagonal (populations, Γ_{jj}) and off-diagonal elements (coherences, Γ_{ij}, $i \neq j$) of the density matrix, and the latter determine the widths of the peaks:

$$R_1(t_1, t_2, t_3) = |V_{10}|^4 e^{+(i\omega_{10} - \Gamma_{10})t_3} e^{-\Gamma_{11} t_2} e^{-(i\omega_{10} + \Gamma_{10})t_1} + |V_{21}|^2 |V_{10}|^2 e^{+(i\omega_{21} - \Gamma_{21})t_3} e^{-\Gamma_{11} t_2} e^{-(i\omega_{10} + \Gamma_{10})t_1} \quad (2a)$$

$$R_2(t_1, t_2, t_3) = |V_{10}|^4 e^{+(i\omega_{10} - \Gamma_{10})t_3} e^{-\Gamma_{11} t_2} e^{+(i\omega_{10} - \Gamma_{10})t_1} + |V_{10}|^2 |V_{21}|^2 e^{+(i\omega_{21} - \Gamma_{21})t_3} e^{-\Gamma_{11} t_2} e^{+(i\omega_{10} - \Gamma_{10})t_1} \quad (2b)$$

$$R_3(t_1, t_2, t_3) = |V_{10}|^4 e^{+(i\omega_{10} - \Gamma_{10})t_3} e^{+(i\omega_{10} - \Gamma_{10})t_1} + |V_{10}|^2 |V_{12}|^2 e^{+(i\omega_{21} - \Gamma_{21})t_3} e^{+(i\omega_{20} - \Gamma_{20})t_2} \times e^{+(i\omega_{10} - \Gamma_{10})t_1} \quad (2c)$$

$$R_4(t_1, t_2, t_3) = |V_{10}|^4 e^{+(i\omega_{10} - \Gamma_{10})t_3} e^{-(i\omega_{10} + \Gamma_{10})t_1} + |V_{10}|^2 |V_{12}|^2 e^{+(i\omega_{10} - \Gamma_{10})t_3} e^{-(i\omega_{20} + \Gamma_{20})t_2} \times e^{-(i\omega_{10} + \Gamma_{10})t_1} \quad (2d)$$

In the case of 2D-IR spectroscopy, the rephasing and non-rephasing contributions to the spectrum are computed as follows:

$$S_{\mathrm{NR}} = \mathrm{Re} \int_0^\infty \mathrm{d}t_3 e^{i\omega_3 t_3} \int_0^\infty \mathrm{d}t_1 e^{i\omega_1 t_1} [R_1 + R_4] \quad (3)$$

$$S_{\mathrm{R}} = \mathrm{Re} \int_0^\infty \mathrm{d}t_3 e^{i\omega_3 t_3} \int_0^\infty \mathrm{d}t_1 e^{i\omega_1 t_1} [R_2 + R_3] \quad (4)$$

It is important to note that as third-order processes, 2D-IR and vibrational echo spectroscopy can only access first and second excited vibrational levels when starting in the ground state. In the present model, we set the anharmonicity ($\omega_{01} - \omega_{12}$) to 10 cm^{-1}, a typical value for terminal CO stretching modes in metal carbonyls, and we also assume harmonic scaling of the transition dipole moments. To compute a homodyne-detected DVE signal spectrum from the above equations, one sets t_1 and t_2 to zero and computes the modulus square polarization in the frequency domain:

$$P^{(3)}_{\mathrm{DVE}}(t) = \int_0^\infty \mathrm{d}t_3 S^{(3)} E_3(t - t_3) E_2(t - t_3) E_1(t - t_3) \quad (5)$$

$$I_{\mathrm{DVE}}(\omega) \propto \left| \int_0^\infty e^{i\omega t} P^{(3)}_{\mathrm{DVE}}(t) \mathrm{d}t \right|^2 \quad (6)$$

To obtain a transient-DVE difference spectrum, two signals are generated corresponding to the equilibrium and non-equilibrium concentrations of molecules, and the difference in signal intensity is computed. In the present paper we are principally concerned with the transient-DVE signal arising from the depletion of the parent species (described below) and ignore the photoproduct response because it does not overlap the parent. The present model only includes the signal arising from the parent molecules, but it can be easily extended to treat a mixture of different molecules, such as other isomers and the photoproducts, including their equilibrium and non-equilibrium populations, by simply adding multiple response functions with different sets of parameters. In the above equations, the induced polarization scales linearly with respect to the number of oscillators (molecules), and the signal intensity scales with the square of the number of molecules. This nonlinear scaling makes the extraction of kinetic information from a t-DVE experiment somewhat cumbersome compared to a transient absorption measurement where the signal intensity scales linearly with respect to the number of oscillators. In the next section we derive the kinetic equations for analyzing t-DVE traces and explore the implications of making simplifications in the data analysis.

The absorption spectrum can similarly be computed from the linear response function, $J(t)$, where

$$J^{(1)}(t) = |V_{10}|^2 e^{-(i\omega_{10} + \Gamma_{10})t} \quad (7)$$

which leads to the first-order induced polarization $P^{(1)}(t)$:

$$P^{(1)}(t) = \int_0^\infty J^{(1)} E_t(t - \tau) \mathrm{d}\tau \quad (8)$$

Note that since, within the current treatment, linear spectroscopy can only access the first-excited state, the optical response

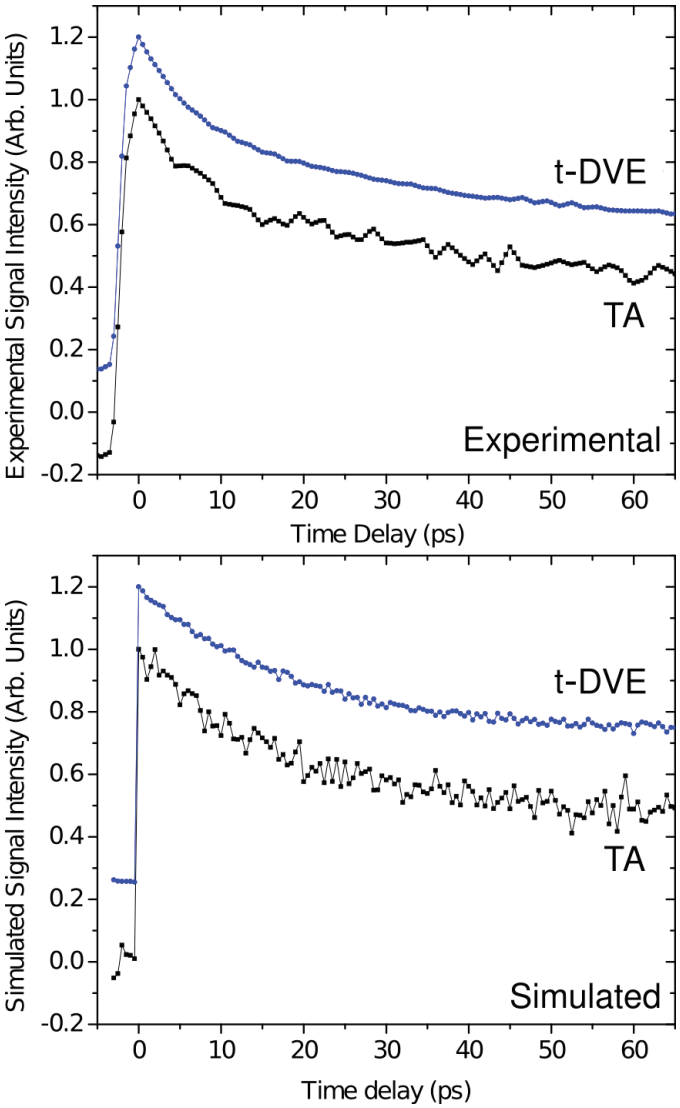

FIG. 2. (**Top**) Experimental and (**bottom**) simulated transient DVE and transient absorption traces. The experimental traces were collected back to back under identical conditions, and the simulated plots were obtained using the same laser noise and excitation ratios for both curves. The experimental curves are obtained by averaging 1000 laser shots (10×100-shot window) per point, or a total data acquisition time of approximately 300 seconds. The two curves are offset for clarity.

of an (an)harmonic oscillator is identical to that of a two-level system.

The detected infrared pulse spectrum (after passing through the sample) can be computed as an interference between the radiated field, E_{induced}, arising from the induced linear polarization[†] and the probe pulse field itself.

$$I_{\text{Abs}}(\omega) = \left| \int_0^\infty [E_{\text{Induced}}(t) - E_t(t)] e^{i\omega t} \mathrm{d}t \right|^2 \qquad (9)$$

To gain a better understanding of the experimental measurements outlined below, we use these models to compute the transient-absorption and transient-DVE signals as a function of the number of oscillators, or concentration of molecules, and explore the signal-to-noise ratio dependence of the computed signals on the laser and detector noise. The time-dependent difference TA and t-DVE traces (Fig. 2) are simulated by generating signals corresponding to two different populations—pumped and unpumped—at various delays after the phototrigger. The evolution of the transient population after the UV excitation is modeled using a single-exponential function with values that closely match the experimental conditions: 10% excitation fraction, 18 ps recombination lifetime, and 50% rebinding ratio.

EXPERIMENTAL METHODS AND RESULTS

The ultrafast optical setup has been described in detail elsewhere.[30,44] In brief, an 800-nm Ti : Sapphire regenerative amplifier (Spectra Physics Spitfire Pro) pumps a BBO-based dual-OPA system, which is then used to generate mid-IR in GaSe by difference frequency generation between the OPA signal and idler. The First OPA/DFG setup is used to generate pump pulses E_1 and E_2, whereas the second setup generates E_3 and E_t. The last beam E_t is used for alignment and acts as the probe in transient-absorption measurements. A measurement of the IR pulse fluctuations shows that these fluctuations (Gaussian white noise) on the two OPA/DFG setups are essentially uncorrelated. Given that the same white light source is used to seed both OPAs, the lack of correlation in their outputs suggests that fluctuations in the white light are irrelevant, indicating that the nonlinear OPA process is being saturated. The IR beams are arranged in a box geometry and the signal spectrum is detected by upconversion into the visible with a 300-ps highly chirped pulse derived from the amplifier output before compression.[45] The visible spectrum is detected using 20 rows (vertically binned) of a 1340-by-100-pixel charge-coupled device (CCD) detector attached to a conventional grating spectrometer. Chirped-pulse upconversion allows us to use a silicon-based detector, and thus affords improved detection sensitivity and lower noise levels. Part of the 800-nm amplifier output is frequency-doubled in a 0.4-mm BBO crystal to obtain a 400-nm phototrigger pulse. The UV pulse is chopped at half the laser repetition rate of 1 kHz, and the UV-IR delay is scanned continuously while the signal spectrum (absorption or DVE) is measured at the laser repetition rate. The difference signal is computed at varying delays using an integration window of 100 pulses, giving an effective UV-IR time resolution of ~500 fs.

The test molecule used for the experiments is cyclopentadienylmolybdenum(II) tricarbonyl dimer, a complex which upon excitation at 400 nm undergoes metal–metal bond cleavage to generate solvent-caged monomer radicals.[39] This particular molecule is chosen because of the large nonlinear signal inherent to metal carbonyls and because the in-cage recombination to cage escape ratio is large, making it an ideal test case for comparing the kinetics measured with t-DVE and TA. The sample solution in ethyl acetate is flowed in a 200-μm-path-length flow cell equipped with 2-mm calcium fluoride windows using a peristaltic pump. In addition, the sample cell is mechanically moved to minimize scattering caused by the accumulation of a photoproduct on the cell windows. The solute concentration is adjusted to yield a ~50% transmittance at the main infrared absorption band at 1958 cm^{-1}, which corresponds to a concentration of approximately 2.6 mM. The corresponding extinction coefficients for the two transitions are

[†] The radiated field is proportional to the induced polarization. A full derivation of these equations is given in Ref. 43.

1437 m^2/mole and 800 m^2/mole at 400 nm and at 1958 cm^{-1}, respectively. The optical density of the sample at 400 nm is ~0.4, and the UV energy is adjusted to yield an excitation fraction of approximately 0.1 (ratio of excited to ground-state molecules following absorption of the UV pulse). About 50% of the radicals undergo geminate recombination inside the solvent cage with a time constant of ~16 ps and the rest diffuse into the bulk solution.[37] To monitor the cage-recombination kinetics, an absorption peak at 1958 cm^{-1} corresponding to the dimer is monitored as a function of time delay after ultraviolet excitation. This peak exhibits a bleach upon absorption of 400-nm light as the population of dimer molecules is depleted; a bleach recovery is observed as the product molecules (monomers) recombine to repopulate the parent states. To obtain a kinetic trace (Fig. 2) the t-DVE or TA signals are integrated over the width of the peak.

ESTIMATION OF SIGNAL-TO-NOISE RATIOS

Transient-DVE is a background free experiment; therefore, the signal-to-noise ratio (SNR) is significantly improved in comparison with transient absorption. The noise percentage for t-DVE measurements will depend mainly on the laser fluctuations, signal intensity, and the excitation fraction. Assuming that the experiments are carried out in the regime where the signal intensity is large enough so that the detector noise can be neglected, and also assuming negligible fluctuations in the trigger pulse, the SNR for a single pair of shots, or adjacent pulses in the pulse train, can be estimated from the IR pulse fluctuations. As shown in Eq. 10 below, the intensity of the DVE signal is proportional to the square of the three incoming fields:

$$I_{\mathrm{DVE}} \propto (E_1 E_2 E_3)^2 \tag{10}$$

This allows us to compute the fluctuations in the t-DVE signal from the laser intensity fluctuations. In the analysis below we assume that fields E_1 and E_2 have perfectly correlated noise fluctuations and that field E_3 has independent fluctuations as the first two pulses are generated by the same OPA/DFG setup, whereas the third pulse is generated by a second OPA/DFG. We also assume that all three pulses have the same amplitude noise percentage (NP) fluctuations corresponding to Gaussian white noise, denoted σ. In our experimental setup a typical value for NP of the shot-to-shot amplitude fluctuations is $(\sigma/I) = 0.7\%$. The percentage intensity fluctuations of the DVE signal intensity can be computed from the simple equations used to describe the propagation of error in experimental measurements:

$$\sigma_{I_{\mathrm{DVE}}} = 2\sqrt{(2\sigma)^2 + \sigma^2} = \sqrt{20}\sigma \tag{11}$$

The noise percentage for a single pulse-pair difference DVE ($\Delta I_{\mathrm{DVE}} = I_{\mathrm{DVE,Pumped}} - I_{\mathrm{DVE,Unpumped}}$) can be computed as follows:

$$\sigma_{\Delta I_{\mathrm{DVE}}} = \frac{\sqrt{(\sigma_{I_{\mathrm{DVE}}} I_{\mathrm{DVE,Pumped}})^2 + (\sigma_{I_{\mathrm{DVE}}} I_{\mathrm{DVE,Unpumped}})^2}}{I_{\mathrm{DVE,Unpumped}} - I_{\mathrm{DVE,Pumped}}} \tag{12}$$

$$\sigma_{\Delta I_{\mathrm{DVE}}} = \frac{\sigma_{I_{\mathrm{DVE}}} \sqrt{20[(1-\kappa_{\mathrm{exc}})^4 + 1]}}{1 - (1-\kappa_{\mathrm{exc}})^2} \tag{13}$$

In the above equation, κ_{exc} represents the fraction of molecules excited by the trigger pulse. To obtain a simple form of the next equation, we now assume zero correlation in the fluctuations between the difference DVE and the DVE signal itself. This assumption gives an upper limit for the noise estimate:

$$\sigma_{\mathrm{tDVE}} \approx \sqrt{\sigma^2_{\Delta I_{\mathrm{DVE}}} + \sigma^2_{I_{\mathrm{DVE}}}} \tag{14}$$

Using typical values for the present experiment, $(\sigma/I) = 0.7\%$ and $\kappa_{\mathrm{exc}} = 10\%$, gives a Gaussian noise width of ~1.6% with a 100-pulse-pair integration window.

We estimate the noise percentage for transient absorption. We can estimate the noise obtained from subtracting two subsequent laser shots using the following relation:

$$\sigma_{\mathrm{Diff}} = \frac{\sqrt{(I_{\mathrm{Pump}}\sigma_{\mathrm{Pump}})^2 + (I_{\mathrm{Probe}}\sigma_{\mathrm{Probe}})^2}}{I_{\mathrm{Pump}} - I_{\mathrm{Probe}}} \tag{15}$$

In the above equations we assume that there is no correlation between the pulse difference and the normalizing probe pulse. Because the error added by normalizing is negligible compared to the error of the difference between two shots, a good estimate in the error can be obtained from inputting our parameters into Eq. 15:

$$\sigma_{\mathrm{TA}} \approx 2\sigma \frac{\sqrt{(1 - A\kappa_{\mathrm{exc}})^2 + 1}}{A\kappa_{\mathrm{exc}}} \tag{16}$$

Once again, κ_{exc} represents the fraction of molecules excited by the phototrigger, and A corresponds to the fraction of light absorbed by the sample at the frequency of interest. Similar to t-DVE, the TA difference signal is calculated as $(A_{\mathrm{Pumped}} - A_{\mathrm{Unpumped}})/A_{\mathrm{Unpumped}}$. The calculated noise percentage using the same values as above is ~3.9%. From these results we can observe that, under the same experimental conditions, the amount of signal averaging required to obtain the same signal-to-noise ratio with TA as obtained with t-DVE is approximately six times greater assuming a square-root dependence on the number of measurements.

The observation that a higher order spectroscopy method offers signal-to-noise ratio advantages over lower-order approaches is not new and forms the basis for interest in using coherent anti-Stokes Raman spectroscopy (CARS) instead of spontaneous Raman spectroscopy. Under conditions that correspond to typical spectroscopic applications, such as high laser pulse intensity and high oscillator number density, CARS clearly offers significant advantages over incoherent Raman spectroscopy.[46,47] On the other hand, when pulse energy is low—as is required to avoid cell death and tissue damage—and number density is low, Raman actually offers superior signal amplitude and thus enhanced signal-to-noise ratio since the method is linear in the incident intensity.[46]

EXTRACTING KINETICS FROM TRANSIENT DISPERSED VIBRATIONAL ECHO EXPERIMENTS

In this section we derive the equations used for analyzing the transient-DVE signal as a function of the time delay following

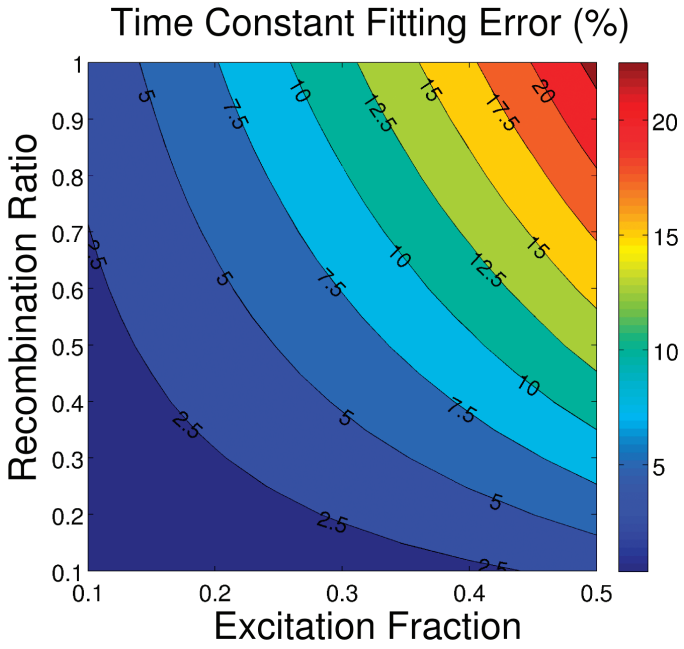

FIG. 3. Error in the recombination time constant obtained by fitting Eq. 21 to a single exponential. Small excitation fraction and low recombination rates are favorable to obtain smaller fitting errors.

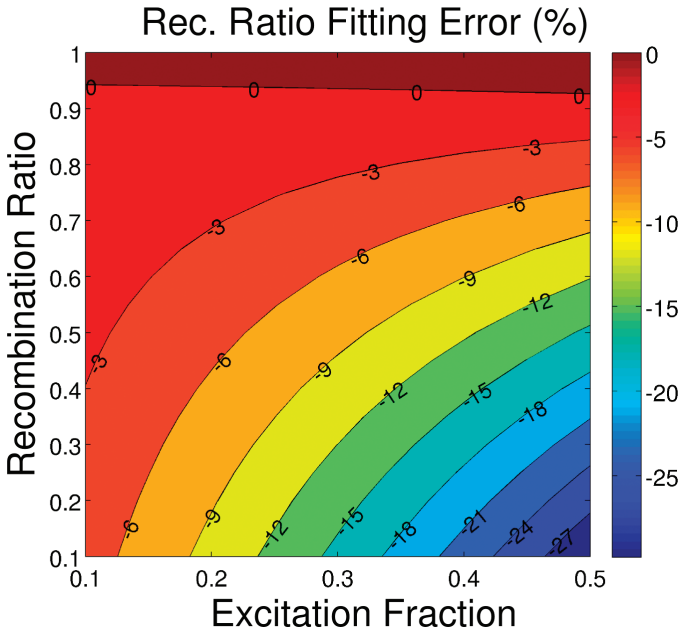

FIG. 4. Error in the recombination ratio (ϕ_{rec}) obtained by fitting Eq. 21 to a single exponential with an offset.

the phototrigger (t). Consider a general reaction of the type:

$$A \underset{k_{rec}}{\overset{h\nu}{\rightleftharpoons}} B \xrightarrow{k_{esc}} C \tag{17}$$

The following equations are derived assuming that the quantity of interest corresponds to the concentration of species A. These equations can be easily modified to represent the quantities of species B or to accommodate other types of reactions. The ratio of equilibrium to transient concentration of A as a function of time after the excitation pulse is described using the following equation:

$$\phi(t) = 1 - [\kappa_{exc}(\phi_{rec}e^{-t/T} - \phi_{rec} + 1)] \tag{18}$$

Where κ_{exc} is the excitation fraction (the fraction of molecules excited by the pump pulse), T is the observed rate of recovery of A, and ϕ_{rec} can be considered a recombination "quantum yield", and it is expressed as:

$$\phi_{rec} = \frac{k_{rec}}{k_{rec} + k_{esc}} \tag{19}$$

Since the DVE intensity is proportional to the square of the number of oscillators at a given frequency (e.g., number of reactant or product molecules, in this particular case reactant molecules), the transient signal can be calculated as follows:

$$I_{tDVE}(t) = \frac{I_{Pumped} - I_{Unpumped}}{I_{Unpumped}} = \phi(t)^2 - 1 \tag{20}$$

Substituting $\phi(t)$ into the above equation yields the following relation:

$$I_{tDVE}(t) = (\kappa_{exc}e^{-2t/T})[e^{t/T}(\phi_{rec} - 1) - \phi_{rec}] \times \{e^{-1t/T}[\kappa_{exc}(\phi_{rec} - 1) + 2] - \kappa_{exc}\phi_{rec}\} \tag{21}$$

Equation 21 represents the t-DVE signal difference in terms of the excitation fraction, the recombination ratio, and the reaction time constant, though fitting an experimentally obtained curve to this equation may be non-trivial despite the mono-exponential underlying kinetics. As seen below, the curves show largely mono-exponential behavior and can be adequately fit to a single exponential curve under many experimentally relevant conditions. Figures 3 and 4 below show the percent error in time constant, T, and recombination ratio, ϕ_{rec}, extracted from a single-exponential fit to generated t-DVE curves. The plots show that the smallest fitting errors are achieved using low excitation ratios and that under these conditions, the errors are small enough that they may be within the normal experimental error. A special case of Eq. 21 can be obtained when the recombination ratio is unity: $\phi_{rec} = 1$. This case applies to a wide range of photophysical reactions in which the system cycles on the same timescale as the experiment:

$$I_{tDVE,\phi_{rec}=1} = \kappa_{exc}e^{-2t/T}(-2e^{t/T} + \kappa_{exc}) \tag{22}$$

Although this relation is simpler than the equation for the general case (Eq. 21), a double-exponential is still required to fit the data. The errors in the recombination time constant obtained by fitting to a single exponential for this case are also shown in Fig. 3. The plot shows that these errors can vary between 5 and 20% depending on the fraction of molecules excited by the pump pulse.

DISCUSSION

In the present experiment we monitor the repopulation of parent molecules using the two described probing techniques. To ensure consistency, both experiments were collected consecutively with no realignment of the optical setup. The experimental traces (Fig. 2) show an initial transient signal arising at zero-time and recovering to approximately 50% of the initial value. The onset of the signal is limited by the experimental time resolution of ~500 fs, which is given by the

size of the integration window (100 shots). A greater time resolution can be achieved using the more standard approach of stepping the UV delay and collecting t-DVE spectra at the various delays. A comparison between the experimental and calculated t-DVE and TA traces (Fig. 2) shows that the signal-to-noise ratios are successfully reproduced using our models. The figures also clearly show that the signal-to-noise ratio is much higher in the t-DVE measurements.

In addition to the signal-to-noise ratio differences it is important to discuss the issue of detection noise. Transient-DVE, a background-free measurement, has an inherent advantage over TA because the signal level can be largely adjusted so that the full dynamic range of the detector is used. Therefore, an improved signal-to-noise ratio and lower averaging times can be realized by this method. Also, unlike TA, small spectral shifts in the laser pulses do not cause large distortions of the background in the difference spectrum. A change in the background as a result of pulse fluctuations can pose a problem when trying to monitor the amplitude of the different features in the spectrum. Many of the limitations of TA outlined in this paper can be overcome by detecting a reference pulse at every laser shot in a dual-detection system as is implemented in many experimental cases. Naturally, this requires multiple detector arrays and a slightly more complicated optical setup, and similar to TA, the signal-to-noise ratio in t-DVE can be greatly improved by referencing. As t-DVE is a background-free signal, small spectral shifts of the Gaussian pump pulses do not have a significant effect on the signal amplitude, and the main source of noise remains the shot-to-shot pulse amplitude fluctuations. Therefore, the signal-to-noise in t-DVE can be greatly improved by detecting the integrated pump pulse intensities with a single-channel detector and normalizing each spectrum by the pump amplitude. It is also important to point out that the present signal-to-noise ratio comparison is carried out on a strongly infrared active terminal carbonyl stretching mode, where the DVE signal can be made to span the full dynamic range of the detector. Therefore, in the models presented, only the laser fluctuations are considered to be a source of measurement noise. Other sources of noise such as detector dark counts, digitization, and shot noise may need to be explicitly considered when measuring weaker transitions.

In principle, t-DVE spectra feature narrower peaks than TA because, due to the four-field interactions, the signal field amplitude for ground-to-first-excited-state transitions scales with the fourth power of the transition dipole moment. However, several contributions from anharmonic states may actually broaden the peaks. The DVE signal contains contributions from excited-state transitions, which have similar line widths, similar intensities, and appear slightly red-shifted with respect to the fundamental transitions as a result of anharmonicity. Although they provide additional information about the system Hamiltonian, these excited-state transitions and combination bands can contribute to broader line shapes in t-DVE compared to TA. If the anharmonicity is large enough compared to the peak widths, the narrower features may be extracted by fitting the DVE line shapes. Because the DVE is a projection of the 2D spectrum, cross-peaks in the 2D spectrum can appear in the DVE signal in different ways. Cross-peaks that arise from excitation and emission in the same manifold, such as the cross-peaks between two different modes (q_1 and q_2, for example), largely serve to amplify the DVE spectrum since they appear at detection frequencies matching the diagonal peaks. Cross-peaks that are explicitly due to anharmonicity—either diagonal (i.e., q_1^3) overtones or off-diagonal (i.e., $q_1 q_2^2$) combination bands—broaden the DVE spectrum because they contribute signal amplitude at frequencies that are different from the diagonal features. In addition to broadening the line shapes, these anharmonic contributions may complicate the interpretation of the DVE spectrum; however, since the DVE signal can be reconstructed from a 2D-IR spectrum, the latter can be used to directly interpret all the peaks in the DVE spectrum. In many systems, the photoexcitation process deposits enough energy into the molecule to significantly raise its temperature, thus leading to broader features at early times.[30,48] Transient-DVE is sensitive to small changes in the molecular structure through the anharmonic couplings and thus it would likely make a sensitive probe of temperature. The effects of dynamics on linear and nonlinear spectral line shapes have been successfully modeled using frequency maps combined with molecular dynamics simulations.[49–52] Recently, Tokmakoff and co-workers have employed DVE spectroscopy to study the unfolding of a protein triggered by a temperature jump.[32,33] Their interpretation of the transient-DVE data is aided by the 2D-IR spectrum of the same system. Finally, the nonlinear intensity scaling with respect to the spectra of the infrared pulses serves to localize the DVE signal in frequency, making TA a better choice for exploring the spectroscopic landscape, followed by DVE "zooms" in specific regions of interest.

The increased sensitivity and lower noise levels in t-DVE come at the cost of more complicated extraction of kinetic data from the experiment. The mono-exponential fitting procedure, as shown in Fig. 3, shows that the error in recovering the underlying mono-exponential rate constant is small as long as the fraction of excited molecules remains small. The actual errors remain within a few percent as long as the excitation fraction remains less than 10%. Equation 21 shows that the observed signal-decay curve is a bi-exponential, where the two exponentials have opposite sign; therefore, a single-exponential fit always gives an upper limit for the underlying kinetic rate of the reaction. Multi-exponential kinetics may further complicate the extraction of lifetimes from t-DVE and would likely require partial knowledge of the reaction along with numerical modeling of the data, a problem that is not present in TA spectroscopy. The plot in Fig. 4 also shows that the offset in the single-exponential fit is a lower limit for the actual recombination ratio. In this context it is important to report the actual geminate rebinding time constant of cyclopentadienylmolybdenum(II) tricarbonyl dimer of 16.18 $\pm$ 0.67 ps (TA), 16.08 $\pm$ 0.38 (t-DVE), and the rebinding ratio of 0.496 $\pm$ 0.08 (TA), 0.51 $\pm$ 0.04 (t-DVE) obtained by fitting a single exponential to the experimental curves in Fig. 2. We would like to point out that these values replace our previously reported time constant of 31 ps in an earlier publication,[37] where the measured lifetime of 15.6 ps was doubled based on a simplistic consideration of the population dependence of t-DVE.

One final matter that should be discussed in the present context is the issue of orientational relaxation. Transient-DVE, similar to transient-2D-IR, is a fifth-order nonlinear experiment; but because the three pulses are time-coincident, the simpler third-order formalism can be used to analyze the results.[53] This simplification is clearly not valid for transient-2D-IR spectroscopy where the full set of fifth-order tensor elements must be taken into consideration.[54] However, it is important to keep in mind that the contribution from orientational relaxation is not identical to that for TA due to the fact that t-DVE is a nonlinear probe, thus

altering the dependence on the number of oscillators as well as the transition dipole moments involved. The equations provided above for analyzing the signal decay kinetics can be slightly modified to analyze orientational contributions to the t-DVE signal, though such a treatment is beyond the scope of this work. Additional information relating to the molecular Hamiltonian of the transient species, such as the relative orientation of the transition dipoles, can be obtained from a transient-DVE experiment by controlling the polarization of the three probe pulses.[54]

CONCLUSION

We have compared two different spectroscopic techniques used for obtaining kinetic information on non-equilibrium systems: transient-DVE and transient-absorption spectroscopy. We have shown that transient-DVE offers improved signal-to-noise ratios over transient absorption while offering additional structural information that can be related to the molecular Hamiltonian. The results also show that t-DVE can provide reasonably high signal-to-noise ratios while avoiding the need for detecting a reference spectrum at every laser shot. Although the equations associated with modeling the kinetics using a nonlinear probe can become cumbersome, single-exponential fitting of the transient data produces rather accurate estimates of the kinetics, especially under low excitation conditions.

In addition to serving as a probe of molecular kinetics, t-DVE can be directly related to transient-2D-IR experiments by a simple projection on to the detection axis; thus, it may be possible to extract much of the information content in transient-2D-IR using this simpler technique, which may prove useful in situations in which collecting a full 2D-IR of a transient species may not be feasible. Alternatively, one could extract structural information and assign the spectrum using transient-2D-IR spectra at a few time delays and measure the kinetics using t-DVE. Although the t-DVE experiment requires a more complicated optical setup, transient-DVE may become an attractive complement to TA, as has already been demonstrated in studies of temperature-jump protein folding[29,33] and ultrafast photochemistry.[34]

ACKNOWLEDGMENTS

We thank Professor Eitan Geva for the insightful discussions. This work is supported by the National Science Foundation (CHE-0748501) and by an Excellence in Research Fellowship from the University of Michigan (C.R.B.).

1. J. Bredenbeck, J. Helbing, J. Kumita, G. Woolley, and P. Hamm, Proc. Nat. Acad. Sci. U.S.A. **102,** 2379 (2005).
2. P. Hamm, J. Helbing, and J. Bredenbeck, Annu. Rev. Phys. Chem. **59,** 291 (2008).
3. T. Elsaesser, Acc. Chem. Res. **42,** 1220 (2009).
4. J. R. Dwyer, J. Dreyer, E. T. J. Nibbering, and T. Elsaesser, Chem. Phys. Lett. **432,** 146 (2006).
5. K. Heyne, N. Huse, J. Dreyer, E. T. J. Nibbering, T. Elsaesser, and S. Mukamel, J. Chem. Phys. **121,** 902 (2004).
6. P. B. Petersen, S. T. Roberts, K. Ramasesha, D. G. Nocera, and A. Tokmakoff, J. Phys. Chem. B **112,** 13167 (2008).
7. S. T. Roberts, K. Ramasesha, and A. Tokmakoff, Acc. Chem. Res. **42,** 1239 (2009).
8. P. A. Anfinrud, C. Han, and R. M. Hochstrasser, Proc. Nat. Acad. Sci. U.S.A. **86,** 8387 (1989).
9. M. H. Lim, T. A. Jackson, and P. A. Anfinrud, Nature Struct. Biol. **4,** 209 (1997).
10. J. Bredenbeck, J. Helbing, K. Nienhaus, G. U. Nienhaus, and P. Hamm, Proc. Nat. Acad. Sci. U.S.A. **104,** 14243 (2007).
11. K. Wynne and R. M. Hochstrasser, Chem. Phys. **193,** 211 (1995).
12. S. Woutersen, U. Emmerichs, and H. J. Bakker, Science (Washington, D.C.) **278,** 658 (1997).
13. H. J. Bakker, S. Woutersen, and H. K. Nienhuys, Chem. Phys. **258,** 233 (2000).
14. M. Cho, Chem. Rev. **108,** 1331 (2008).
15. M. D. Fayer, Annu. Rev. Phys. Chem. **60,** 21 (2009).
16. J. P. Oglivie and K. J. Kubarych, Adv. At. Mol. Opt. Phy. **57,** 249 (2009).
17. P. Hamm, M. H. Lim, and R. M. Hochstrasser, J. Phys. Chem. B **102,** 6123 (1998).
18. C. R. Baiz, P. L. McRobbie, N. K. Preketes, K. J. Kubarych, and E. Geva, J. Phys. Chem. A **113,** 9617 (2009).
19. C. R. Baiz, P. L. McRobbie, J. M. Anna, E. Geva, and K. J. Kubarych, Acc. Chem. Res. **42,** 1395 (2009).
20. A. M. Moran, J. Dreyer, and S. Mukamel, J. Chem. Phys. **118,** 1347 (2003).
21. N. Demirdoven, M. Khalil, O. Golonzka, and A. Tokmakoff, J. Phys. Chem. A **105,** 8025 (2001).
22. N. Demirdoven, M. Khalil, and A. Tokmakoff, Phys. Rev. Lett. **89,** 237401 (2002).
23. M. Khalil, N. Demirdoven, and A. Tokmakoff, J. Phys. Chem. A **107,** 5258 (2003).
24. J. Zheng, K. Kwak, J. Asbury, X. Chen, I. Piletic, and M. Fayer, Science (Washington, D.C.) **309,** 1338 (2005).
25. A. V. Pakoulev, M. A. Rickard, K. M. Kornau, N. A. Mathew, L. A. Yurs, S. B. Block, and J. C. Wright, Acc. Chem. Res. **42,** 1310 (2009).
26. F. Fournier, R. Guo, E. M. Gardner, P. M. Donaldson, C. Loeffeld, I. R. Gould, K. R. Willison, and D. R. Klug, Acc. Chem. Res. **42,** 1322 (2009).
27. F. Fournier, E. M. Gardner, D. A. Kedra, P. M. Donaldson, R. Guo, S. A. Butcher, I. R. Gould, K. R. Willison, and D. R. Klug, Proc. Nat. Acad. Sci. U.S.A. **105,** 15352 (2008).
28. J. Bredenbeck, J. Helbing, and P. Hamm, J. Am. Chem. Soc. **126,** 990 (2004).
29. J. Bredenbeck, J. Helbing, R. Behrendt, C. Renner, L. Moroder, J. Wachtveitl, and P. Hamm, J. Phys. Chem. B **107,** 8654 (2003).
30. C. R. Baiz, R. McCanne, M. J. Nee, and K. J. Kubarych, J. Phys. Chem. A **113,** 8907 (2009).
31. W. Xiong, J. E. Laaser, P. Paoprasert, R. A. Franking, R. J. Hamers, P. Gopalan, and M. T. Zanni, J. Am. Chem. Soc. **131,** 18040 (2009).
32. A. W. Smith and A. Tokmakoff, Angew. Chem. Int. Ed. **46,** 7984 (2007).
33. H. S. Chung, M. Khalil, and A. Tokmakoff, J. Phys. Chem. B **108,** 15332 (2004).
34. K. D. Rector, D. Zimdars, and M. D. Fayer, J. Chem. Phys. **109,** 5455 (1998).
35. V. Cervetto, J. Helbing, J. Bredenbeck, and P. Hamm, J. Chem. Phys. **121,** 5935 (2004).
36. K. C. Jones, Z. Ganim, and A. Tokmakoff, J. Phys. Chem. A **113,** 14060 (2009).
37. C. R. Baiz, R. McCanne, and K. J. Kubarych, J. Am. Chem. Soc. **131,** 13590 (2009).
38. J. C. Linehan, C. R. Yonker, R. S. Addleman, S. T. Autrey, J. T. Bays, T. E. Bitterwolf, and J. L. Daschbach, Organometallics **20,** 401 (2001).
39. T. E. Bitterwolf, Coord. Chem. Rev. **211,** 235 (2001).
40. A. B. Oelkers, L. F. Scatena, and D. R. Tyler, J. Phys. Chem. A **111,** 5353 (2007).
41. A. B. Oelkers, E. J. Schutte, and D. R. Tyler, Photochem. Photobiol. Sci. **7,** 228 (2008).
42. Y. Tanimura and A. Ishizaki, Acc. Chem. Res. **42,** 1270 (2009).
43. S. Mukamel, *Principles of Nonlinear Optical Spectroscopy* (Oxford University Press, New York, 1995).
44. C. Baiz, M. Nee, R. McCanne, and K. Kubarych, Opt. Lett. **33,** 2533 (2008).
45. M. J. Nee, R. McCanne, K. J. Kubarych, and M. Joffre, Opt. Lett. **32,** 713 (2007).
46. M. Cui, B. R. Bachler, and J. P. Ogilvie, Opt. Lett. **34,** 773 (2009).
47. G. I. Petrov, R. Arora, V. V. Yakovlev, X. Wang, A. V. Sokolov, and M. O. Scully, Proc. Nat. Acad. Sci. U.S.A. **104,** 7776 (2007).
48. D. A. Steinhurst, A. P. Baronavski, and J. C. Owrutsky, Chem. Phys. Lett. **361,** 513 (2002).
49. K.-I. Oh, J.-H. Choi, J.-H. Lee, J.-B. Han, H. Lee, and M. Cho, J. Chem. Phys. **128,** 154504 (2008).
50. J. Asbury, T. Steinel, C. Stromberg, S. Corcelli, C. Lawrence, J. Skinner, and M. Fayer, J. Phys. Chem. A **108,** 1107 (2004).
51. S. A. Corcelli, C. P. Lawrence, and J. L. Skinner, J. Chem. Phys. **120,** 8107 (2004).
52. B. A. Lindquist, K. E. Furse, and S. A. Corcelli, Phys. Chem. Chem. Phys. **11,** 8119 (2009).
53. A. Tokmakoff, J. Chem. Phys. **105,** 1 (1996).
54. J. Bredenbeck, J. Helbing, and P. Hamm, J. Chem. Phys. **121,** 5943 (2004).